sustainability

MDPI

Article

Leaching Study of Guinean Bauxite Tailings in aqueous HCl Solution for the Extraction of Aluminum

Maria Bagani [1,*], Dimitrios Kotsanis [1], Michalis Vafeias [1,*], Anastasia Pilichou [1], Efthymios Balomenos [2] and Dimitrios Panias [1]

[1] School of Mining and Metallurgical Engineering, National Technical University of Athens, 15780 Athens, Greece; dkotsanis@metal.ntua.gr (D.K.); anastasiapilihou@gmail.com (A.P.); panias@metal.ntua.gr (D.P.)

[2] Mytilineos SA-Metallurgy Business Unit, Alumina and AluminumPlant, St. Nikolas, 32003 Paralia Distomou, Greece

* Correspondence: e: mariampagani@mail.ntua.gr (M.B.); michalisvafeias@mail.ntua.gr (M.V.); Tel.: +30-21-0772-2177 (M.B.)

Abstract: Primary aluminum production is dependent on the Bayer process for Al_2O_3 refining and the Hall–Héroult process for Al production. Both these processes face serious sustainability challenges, while the overall Al supply chain is inflexible and prone to disruptions. One solution to the aforementioned challenges is the adoption of alternative Al_2O_3 production processes from a variety of primary and secondary raw materials. This research paper explores the potential use of bauxite tailings as an alternative secondary resource for alumina production, with an aqueous HCl process technology. Bauxite tailings are solid waste produced during the mining and beneficiation of certain bauxites before their digestion in the Bayer process. The research was conducted in two stages. Initially, 24 h trials using aqueous 5.9 M HCl solution and a 5:100 g/mL solid-to-liquid (S/L) ratio revealed complete dissolution of Al and near-complete dissolution of Fe. In the second stage, investigations involving higher S/L ratios under the same conditions confirmed that an S/L ratio of 20:100 g/mL represented the optimal parameters for bauxite tailings leaching, producing a 36.8 g/L Al and 25.2 g/L Fe concentration solutions. The PLS produced under the optimum conditions is suitable for downstream processing for the production of $AlCl_3 \cdot 6H_2O$.

Keywords: alumina leaching; bauxite tailings; sustainable alumina production; alternative alumina resources

Citation: Bagani, M.; Kotsanis, D.; Vafeias, M.; Pilichou, A.; Balomenos, E.; Panias, D. Leaching Study of Guinean Bauxite Tailings in aqueous HCl Solution for the Extraction of Aluminum. *Sustainability* **2023**, *15*, 16232. https://doi.org/10.3390/su152316232

Academic Editor: Francesco Ferella

Received: 3 October 2023
Revised: 14 November 2023
Accepted: 17 November 2023
Published: 23 November 2023

1. Introduction

Primary aluminum production is achieved by the combination of two metallurgical processes: (a) the Bayer process, which refines bauxite to metallurgical-grade alumina (MG-Al_2O_3), and (b) the Hall–Héroult process, which produces aluminum metal by electrolytically reducing MG-Al_2O_3 in a cryolite bath. Increasing the sustainability of both these processes and of the entire primary aluminum supply chain is one of the industry's main challenges in the 21st century.

Concerning the industry's contribution to CO_2 emissions, according to the International Energy Agency's (IEA) most recent analysis, the production of aluminum using the current state-of-the-art technologies is a significant source of CO_2, accounting for approximately 270 Mt of direct emissions in 2022 [1]. This accounts for about 3% of the global direct industrial CO_2 emissions. According to the same source, the direct emissions intensity of aluminum production must decline by an annual rate of nearly 4% until 2030, if the goal of net zero emissions is to be met by 2050. Although the major part of these emissions is attributable to the electrolytic reduction of MG-Al_2O_3, the energy demands of the Bayer process are approximately 12.8 MJ per kg of Al_2O_3, and the corresponding CO_2 emissions are 0.83 kg per kg of Al_2O_3 [2].

Aluminum is recognized as an important component for a number of technologies critical to the energy transition, e.g., in lightweight vehicles and solar energy technologies. For this reason, aluminum demand is expected to increase in the next few decades. For instance, Svendrup et al. [3] in their study of the aluminum market's long-term development, suggested that primary production of aluminum will reach its maximum in the coming decades. A. Elshkaki et al. [4] studied the material–energy–water nexus combined with CO_2 emissions for aluminum and developed four global and regional process-based scenarios. Their results indicate that global CO_2 emissions from the production of aluminum will increase, due to increasing demand. Furthermore, this increase is unavoidable even after considering secondary production, energy efficiency, and cleaner energy supply technologies that will be available in the following decades. Similar conclusions are drawn from the study of G. Liu et al. [5], who developed a dynamic material flow analysis model that simulates the future global aluminum cycle. Their model allows for the exploration of emission pathways and mitigation potentials associated with that cycle. Their main finding is that if the aluminum stock patterns of developing countries follow those of the industrialized countries, the target of a 50% emission reduction by 2050 (below 2000 levels) cannot be reached, even when extremely optimistic assumptions for recycling rates and technological breakthroughs are considered.

Concerning the sustainability of the primary aluminum supply chain, its inelastic character has become increasingly apparent in the last few decades. Primary aluminum production depends almost entirely on the supply of bauxite. Specifically, only the high-quality bauxites with an Al_2O_3/SiO_2 mass ratio of at least 7 are appropriate for the Bayer process. Bauxite reserves of such quality are located in specific geographic regions, such as Australia, Guinea, Brazil, Jamaica, China, and India [6]. In the event of regional resource depletion and/or alterations in trade relationships and dependencies (e.g., due to geopolitical, economic, or social factors), the whole supply chain for primary aluminum will be disrupted. For this reason, the EU [7], USA [8], and Canada [9] have labeled bauxite and/or aluminum as critical raw materials.

Finally, focusing specifically on the bauxite mining and refining stages, additional sustainability concerns are raised due to the landfilling of solid wastes from these operations. Bauxite residue, the solid residue remaining after digestion of bauxite is one of the most pressing concerns in the industry. Approximately 0.8–1.5 tonnes of BR are produced per 1 tonne of Al_2O_3 produced in the Bayer process [10]. More recently, attention has been drawn to the solid waste produced during the mining and beneficiation processes of certain bauxite sources. These wastes are termed bauxite tailings (BTs). For instance, it is estimated that for Chinese bauxite, approximately 0.45 t of BTs is produced per tonne of Al_2O_3 [11]

The issue of BTs management has only recently emerged as an additional environmental and sustainability concern [12] due to the increasing importance of bauxite beneficiation as a method of reducing the cost of Al_2O_3 refining. The latter is dependent on the amount of makeup NaOH per ton of Al_2O_3 produced, and bauxites with a ratio of available alumina (AA)/reactive silica (RS) greater than 10 are found to be economically attractive [13]. Hence, the main objective of bauxite beneficiation is to lower the concentration of reactive silica (usually found in the form of kaolinitic clay). Additional beneficiation objectives include reduction in the iron content, particularly in the form of goethite, and reduction in the organic carbon content [14]. As expected, the composition of BTs depends on the composition of the original bauxite. For example, BTs from Chinese karst bauxites are predominantly of aluminosilicate composition, while BTs from lateritic bauxites, such as those originating from Guinea, are richer in iron oxides.

Production of Al_2O_3 from alternative raw materials, both primary and secondary, can significantly contribute to increasing the sustainability of primary aluminum production. The inclusion of alternative Al_2O_3 sources will diversify the supply chain, thus minimizing the risk of disruptions and increasing the strategic autonomy of aluminum metal for nations that do not produce bauxite. Moreover, reducing dependency on bauxite also reduces the accumulation of large volumes of the solid wastes mentioned earlier.

Nowadays, there is significant ongoing research in the field of utilizing alternative raw materials to produce Al_2O_3. Numerous studies have been conducted, with a particular focus on the use of abundant clays (e.g., kaolinitic clays). Many of these studies involve a pretreatment-calcination step before leaching [15,16]. Additionally, investigations are being carried out on the utilization of industrial byproducts such as coal fly ash [17]. Furthermore, efforts are being made to explore the processing of bauxite deposits that are unsuitable for the Bayer process [18]. A study performed by Zhao [19] states that advances in acid treatment in comparison with the Bayer process for low-grade gibbsite bauxite samples suggest treatment with a high molarity HCl solution (10% w/w) for a retention time of 2 h at a temperature of 100 °C. This trial results in over 95% dissolution degree of both Al and Fe and the production of a high silica residue that is easily filtered.

At the forefront of EU research initiatives in the field of alternative technologies for Al_2O_3 production is the AlSiCal project [20]. AlSiCal is developing an integrated process for producing alumina, silica, and calcium carbonate from primary and secondary alternative sources of Al_2O_3. A generic process flowsheet of the AlSiCal technology is shown in Figure 1 and consists of a leaching stage with aqueous HCl as the leaching agent, followed by a precipitation stage whereby aluminum is separated from the solution in the form of $AlCl_3 \cdot 6H_2O$. Finally, a calcination stage leads to the production of Al_2O_3 and allows for HCI recovery. The AlSiCal technology has been tested on a variety of primary raw materials, including anorthosite [21], kaolin [22], and industrial or mining tailings of aluminosilicate composition, e.g., nepheline syenite [23]. The present research work is concerned with the application of the AlSiCal technology to lateritic BTs from Guinea with the principal objective being the effective separation of the Al_2O_3 content from the SiO_2 content. The research is important; currently there have been no attempts to metallurgically valorize this category of BTs (high Fe_2O_3/Al_2O_3 tailings). On the other hand, attempts for the valorization or utilization of the Chinese BTs (high in Al_2O_3/SiO_2 tailings) have been numerous in the last 15 years.

In more detail, W. Yuhua et al. used BTs, unmodified (as is) and modified with $FeCl_3 \cdot 6H_2O$, as adsorbents for Cr(IV) from aqueous solutions [24]. They reported a maximum removal rate of 99.3% for Cr(IV) in the case of the modified material. D. Yang et al. attempted to produce a primary Al-Si alloy from BTs by a carbothermal reduction process [25]. At the optimum condition (pressure 0.1 MPa, maximum temperature 1900 °C, duration 1 h) they managed to obtain an alloy containing a high Al Al-Si-Fe alloy and several carbides of Si and Al. Production of several zeolite precursors from BTs has been achieved, notably 4A Zeolite [26,27], Zeolite, X. [28], and Zeolite, Y. [29]. Y. Peng et al. have studied the use of BT as filler for foamed-mixture lightweight soil with promising results [30,31]. L. Yang et al. concluded that BTs are a suitable raw material for the production of lightweight aggregates (LWA), due to their high concentration of glass-forming oxides [32]. On the other hand, LWA produced from BTs have no expanding capacity, and the addition of CaF_2 or $CaCO_3$ is needed to increase their pore size. Y. Ren et al. prepared high-strength ferric-rich ceramics from BTs at low sintering temperature [33]. For the ceramics produced under the optimum conditions (sintering temperature of 1130 °C), they report a 4.65% breakage ratio under 52 MPa and an apparent density equal to 2.78 g/cm^3. X. Shen et al. suggest that BTs can be used for the production of mullite ($Al_6Si_2O_{13}$) after removal of Fe_2O_3 and K_2O that act as impurities [11]. They studied a combined calcination and acid leaching process with HCl but could not achieve complete removal of Fe and K. Finally, Y. Zhang et al. studied Li-enriched BTs from the Guiyang City, Guizhou Province, and proposed an acid leaching process for coextraction of Al and Li [34]. By using a mixture of H_2SO_4/H_3PO_4, they managed to extract 88% and 96% of Al and Li, respectively.

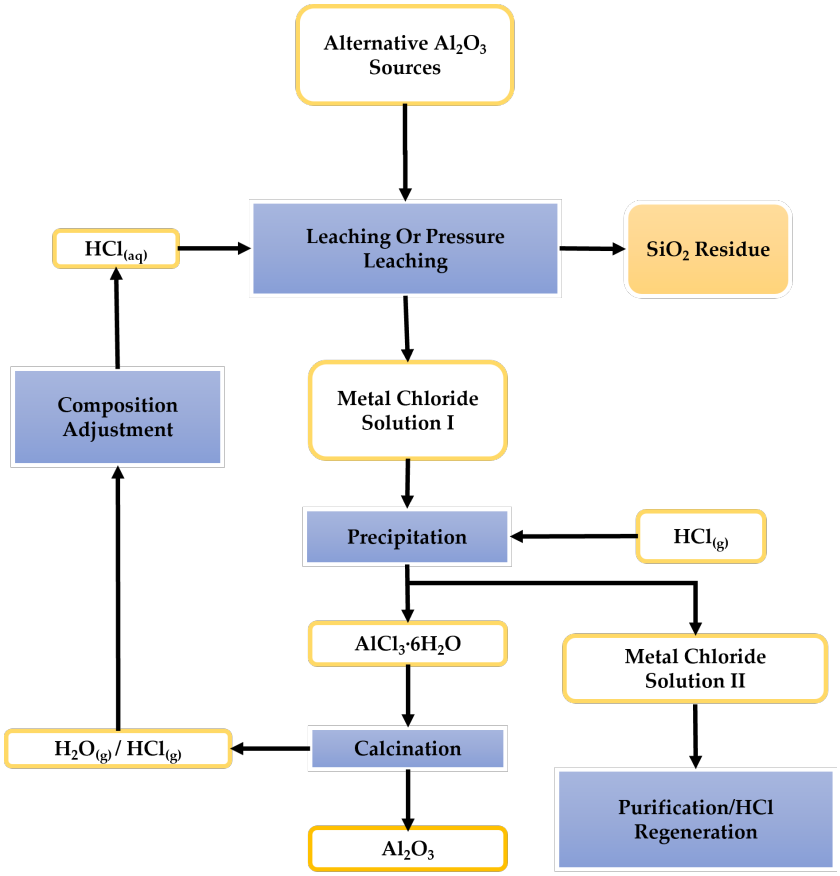

Figure 1. AlSiCal technology generic flowsheet [35].

Thus, the principal aim of this research is to examine Guinean BTs as a raw material for aluminum extraction with an HCl atmospheric pressure leaching process. The process under investigation can be applied to any BTs source of similar composition. Such tailings are abundant in several areas around the globe, where ferruginous karst or lateritic bauxites can be found (Jamaica, Mediterranean, West Africa, etc.) in both active and legacy mining sites.

2. Materials and Methods

2.1. Equipment and Materials Used

2.1.1. Equipment and Chemical Reagents

For the leaching tests, an Amar G 2360 glass reactor was used, equipped with a 1000 mL capacity jacketed glass vessel and a polytetrafluoroethylene (PTFE) lid. A mechanical stirrer is connected to a PLC unit which allows the control of the operating parameters while the heating was controlled by a chiller through the circulation of silicon oil in the external layer of the jacketed vessel. Reagent-grade hydrochloric acid (>37%) and deionized water were mixed for the leaching agent.

Wet chemical analysis of the aqueous solutions produced was carried out using a PinAAcle 900T Atomic Absorption Spectrometer (AAS) and the Inductively Coupled Plasma–Optical Emission Spectrometry (ICP-OES) Optima 8000 by PerkinElmer™ (Waltham, MA, USA). The investigated metals of interest were Al, Fe, Ti, and Si. Calibration standard solutions were prepared from commercially available ICP-OES and AAS standards (1000 ppm) obtained from Merck (Darmstadt, Germany). The standard solutions were prepared in the suitable concentration and diluted further with 1% v/v analytical grade HNO_3 (65%wt.) as required for working standards. High-purity deionized water (18.2 MΩ/cm), and argon (99.999% purity) were used.

To determine the free acidity of the solutions in the presence of hydrolyzable ions, such as Al^{3+} and Fe^{3+}, a sample of the solution is titrated with standard sodium hydroxide solution 1 M (Honeywell) after the metal ions in the solution are masked with EDTA 0.1 mol/L (Chembiotin). Titrations were performed in an auto titrator Model 702 SM manufactured by Metrohm.

The XRD patterns were collected using a MiniFlex 600 benchtop diffractometer (Rigaku, Tokyo, Japan) equipped with a D/tex ultra detector. The diffractometer operated at 40 kV and 15 mA (600 W) with Cu-Kα radiation (Ni-filtered). Diffraction data were collected from 10 to 120° (2θ), in 0.02° (2θ) steps and at a rate of 5° (2θ) per minute. The mineralogical composition of the materials examined was determined using DIFFRAC EVA V5.1 software (Bruker AXS, Karlsruhe, Germany) and the ICDD databases PDF-4+ 2022 and PDF-4 Minerals 2022 [36]. The results of this qualitative analysis are illustrated in Figure 2 and Figures 5 and 7 for the raw and the leached samples, respectively.

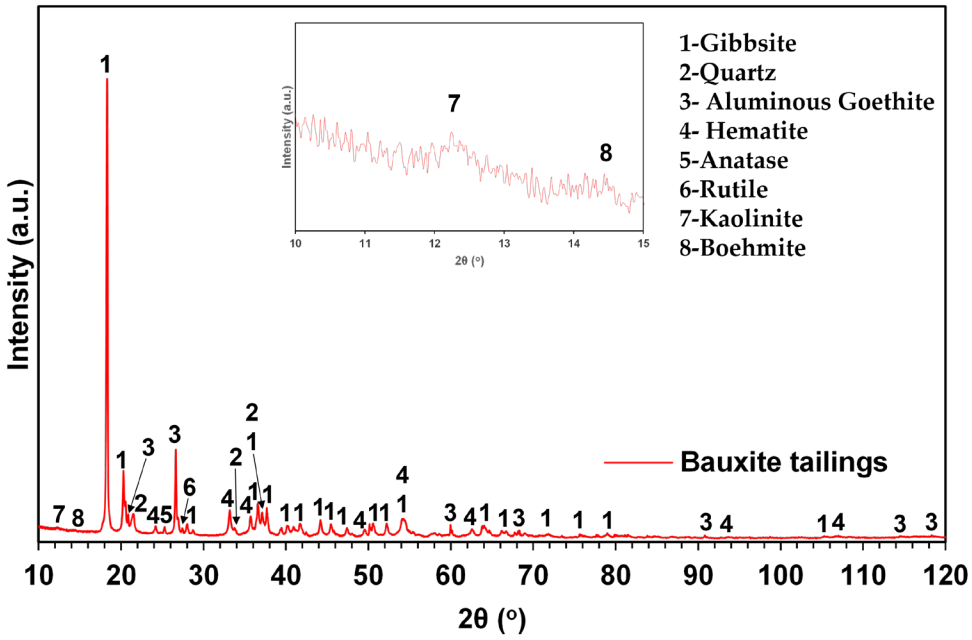

Figure 2. Powder X-ray diffractogram of the bauxite tailings sample used in this study. Legend: 1—Gibbsite, 2—Aluminous Goethite, 3—Quartz, 4—Hematite, 5—Anatase, 6—Rutile, 7—Kaolinite and 8—Boehmite. (The inset in the picture shows the major diffraction peaks of kaolinite and boehmite).

2.1.2. Chemical Analysis of Raw Material

The sample tested in this work originated from the Boffa Prefecture, Guinea. The bauxite from this area contains silica, mainly in the form of quartz. Kaolin is found in trace amounts. Bauxite is sieved and the plus 20 mm particles are sent to alumina refineries whereas the undersized particles (−10 mm), called bauxite tailings, due to their increased silica, cannot be processed by the Bayer process.

The sample of bauxite tailings received was ground to −100 μm. Then, it was dried at 100 °C for 24 h and its chemical composition was determined by wet chemical analysis techniques. The sample was solubilized via the fusion method with a mixture of $Li_2B_4O_7/KNO_3$ at 1000 °C for 1 h and then dissolved in a nitric acid solution. The leaching residue was solubilized via the fusion method with $LiBO_2$ at 1000 °C for 0.5 h and then dissolved in a hydrochloric acid solution. For the determination of loss of ignition content (LOI), 1 gr of the material was calcined at 1000 °C for 1 h. LOI was calculated based on the difference in mass between the starting and calcined material.

The results of the chemical analysis (in equivalent oxide basis) are presented in Table 1.

Table 1. Chemical analysis of the bauxite tailings sample used in this study.

Component	Al_2O_3	Fe_2O_3	SiO_2	TiO_2	LOI	Others
%wt.	38.9 ± 0.3	20.4 ± 0. 3	18.8 ± 0.8	1.5 ± 0.3	19.9 ± 0.5	0.4

The chemical analysis reveals that the raw material used in this study is rich in Al_2O_3 and Fe_2O_3, these two oxides accounting for more ≈than 60% of the raw material. The concentration of SiO_2 is indeed greater compared to bauxites suitable for the Bayer process, and the resulting Al_2O_3/SiO_2 modulus is ≈2.1.

A detailed mineralogical analysis of the material was performed to determine the phase composition of the raw material.

2.1.3. Mineralogical Analysis of Raw Material

The mineralogical analysis of the raw material used in this study is presented in Figure 2.

According to our findings, the main crystalline phases of the raw material are gibbsite ($Al(OH)_3$), aluminous goethite ($Fe_{0.71}Al_{0.29}O(OH)$), quartz (SiO_2), and hematite (Fe_2O_3). Additionally, Ti-bearing minerals in the form of anatase (TiO_2) and rutile (TiO_2), layer silicates in the form of kaolinite ($Al_2Si_2O_5(OH)_4$), and boehmite ($AlO(OH)$) were also detected. To further understand the composition of the raw material and especially the characteristics of the aluminous goethite phases, a quantitative XRD analysis was also performed.

The quantitative analysis of the raw material was based on the fundamental parameter approach [37] and performed in DIFFRAC TOPAS V6 software (Bruker AXS, Karlsruhe, Germany). All of the initial structure models for the identified crystalline phases were retrieved from the ICDD databases PDF-4+ 2022 and PDF-4 Minerals 2022. As part of this analysis, various parameters of these models were allowed to be refined, such as the lattice parameters, the scale factor, the crystalline size (Lorentzian contribution), and the strain in the case of gibbsite and aluminous goethite (Gaussian contribution). Preferred orientation correction for gibbsite peaks was applied using spherical harmonics of the fourth order [38]. The refinement strategy also included a procedure to estimate the substitution of aluminum for iron in goethite, a common feature that occurs in natural goethites, as summarized in Schulz (1984) [39]. For Al-substituted synthetic goethites, Schulz [39] derived a negative linear relationship between the unit-cell edge length *c* and the substitution of Al, which is expressed by Equation (1).

$$\text{mole\%Al} = 1730 - 572c \quad (1)$$

This empirical relationship is also applicable to natural goethites, as shown by Schwertmann and Carlson (1994) [40], and is widely used for the estimation of aluminum substitution in both synthetic and natural goethites [41–44].

Equation (1) was then modified appropriately to be inserted into the quantitative analysis software and used to calculate the aluminum occupancy at the iron site. At the same time, iron occupancy was restricted in such a way that the sum of these values equals 1. Accordingly, goethite in the raw material showed a significant amount of aluminum substitution in the iron site (about 29 mol. %), indicative of a geochemical environment rich in aluminum.

Furthermore, an effort was made to investigate any amorphous content in the raw material. Amorphous phases are very common in natural and synthetic materials, while their significance in many branches of science and engineering has led to the development of various quantification methods. Among them, the internal and the external standard methods, also known as indirect methods, are widely used, and in this case, for bauxite formations, they highlight the existence of amorphous material whose percentage by weight (wt.) can be up to 19% [45–47]. As for this study, the external standard method was adopted, as first described by O'Connor and Raven (1988) [48], also enabled in Topas. For the implementation of this method, a pure Si powder (NIST-SRM 640f) was used.

The results of the quantitative analysis of the raw material are summarized in Table 2, presenting the percentage by weight (wt.) of each phase and its statistical measure of performance (R_{wp}).

Table 2. Quantitative analysis of the raw material.

Phases—wt. (%)									R_{wp} (%)
Gibbsite	Al-goethite	Quartz	Hematite	Anatase	Rutile	Kaolinite	Boehmite	Amorphous	5.4
56.9	15.2	8.8	7.5	1.0	0.8	0.9	0.2	8.8	

Based on this analysis, the main characteristic of the raw material is the abundance of gibbsite, while the phases of Al-substituted goethite, quartz, and hematite are present in lesser amounts. Regarding the remaining accessory minerals, these are present in minor quantities. Furthermore, a small amount of amorphous phase was calculated. Comparing the results of the chemical analysis with those of the quantitative XRD analysis, the main observation concerns the concentration of SiO_2. The %wt. of SiO_2 attributed to the siliceous phases as determined by the quantitative XRD analysis is lower than the corresponding %wt. of SiO_2 determined by the elemental chemical analysis. This is an indication that the amorphous phase could predominantly be of siliceous composition.

2.2. Methodology

The experimental leaching work, at atmospheric pressure, was performed in two stages. First, a study of the leaching system was performed at 90 °C and with a 5:100 g/mL S/L ratio, a 5.9 M solution, and an intensive stirring rate of 300 rpm. These tests were 24 h in duration and samples were drawn at 0.5, 1, 2, 4, 8, and 24 h. The goal for this stage of the work was to determine the leaching rates of the main metal values and draw information on the behavior of Si in the system.

In the second stage, the effect of the S/L ratio was studied and, specifically, the maximum S/L ratio that can be applied for the atmospheric pressure leaching of the raw material under investigation. The values of the S/L ratio tested were 20:100, 22.5:100, and 25:100 g/mL. The basis for the selection of this range in values was the equivalent molar amount of HCl needed for the complete dissolution of the material. In more detail, the exact molar amount of HCl needed for the dissolution of the Al and Fe hydroxides and Fe and Ti oxides present in the raw material was calculated according to the dissolution Equations (2)–(5) shown below.

$$Al(OH)_{3(s)} + 3H^+ \rightarrow Al^{3+}{}_{(aq)} + 3H_2O_{(l)} \quad (2)$$

$$FeO(OH)_{(s)} + 3H^+{}_{(aq)} \rightarrow Fe^{3+}{}_{(aq)} + 2H_2O_{(l)} \quad (3)$$

$$Fe_2O_{3(s)} + 6H^+{}_{(aq)} \rightarrow 2Fe^{3+}{}_{(aq)} + 3H_2O_{(l)} \quad (4)$$

$$TiO_{2(s)} + 4H^+{}_{(aq)} \rightarrow Ti^{4+}{}_{(aq)} + 2H_2O_{(l)} \quad (5)$$

This equivalent amount corresponds approximately to the 22.5:100 g/mL S/L ratio. Consequently, the 20% S/L ratio test corresponds to an 8% molar excess of HCl and the 25:100 g/mL to a 16% excess of bauxite tailings. Although the stoichiometrically required HCl had been calculated, the application of a higher S/L ratio value was possible due to the hydrolysis that occurs for both Al and Fe. More specifically, acidity produced by the hydrolysis reaction of Al and the Fe reaction, presented in Equation (6), generates acidity in the system and enables the application of higher S/L ratios than the theoretical S/L ratios.

$$Me(H_2O)_m^{+n} \rightleftarrows Me(H_2O)_{m-1}^{+n-1} + H^+ \quad (6)$$

where Me: Al or Fe, $1 < n < 3$ and $3 < m < 6$.

All of the aforementioned parameters in the experimental plan are shown in Table 3.

Table 3. Parameters in the experimental plan for the leaching trials.

	Stage	Temperature (°C)	Pressure (atm)	HCl Concentration (M)	Rotation Speed (rpm)	Duration (h)	S/L Ratio (x:100 g/mL)
1.	24 h tests	90	1	5.9	300	24 (intermediate sampling at 0.5, 1, 2, 4, and 8 h)	5
2.	S/L ratio optimization Tests					2	20, 22.5, 25

All experiments were repeated three times, to ensure reproducibility of results. During leaching experiments, the leaching solution was placed in the reactor and heating was applied. When the reactor reached the target temperature, the solid sample was inserted into the reactor, thus signaling the start of the experiment. At the end of the experiment, the leachate was separated from the solid residues via vacuum filtration. The final pregnant liquid solution (PLS) and any intermediate samples were analyzed by AAS and ICP-OES while the residue was dried, and milled, and its mineralogical composition analyzed by X-ray diffraction (XRD).

Equation (7) defines the %wt. dissolution of each metal as its mass dissolved in the PLS, divided by its mass in the solid phase prior to leaching.

$$\text{x dissolution}(\%) = \frac{m_{\text{x dissolved}}}{m_{\text{x BT}}} \times 100 \quad (7)$$

where $m_{\text{x dissolved}}$ is the respective mass of its elements that dissolved in a solution, and $m_{\text{x BT}}$ is the mass of its element that was present in the total amount of BTs that was leached.

3. Result

3.1. Kinetics of Metal Dissolution

As mentioned earlier, experimental work on the leaching behavior of bauxite tailings started with a 24 h leaching test where the effect of time on the dissolution of the major metals was evaluated. The %wt. dissolution rates for Al, Fe, and Ti are shown in Figure 3. The behavior of Si is shown separately in Figure 4. The average %wt. dissolution and concentration of these metals in the PLS as a function of leaching duration are shown in Table 4.

Table 4. Dependence of average metal concentration and %wt. dissolution of Al, Fe, Ti, and Si in the PLS as a function of leaching duration.

Duration (h)	Average Metal Concentration in PLS				Average %wt. Metal Dissolution in PLS			
	Al (g/L)	Fe (g/L)	Ti (mg/L)	Si (mg/L)	Al	Fe	Ti	Si
0.5	8.2	6.2	47.2	79.0	79.6	80.3	9.2	2.4
1	9.1	6.6	51.0	55.0	88.7	86.0	10.0	1.7
2	9.3	6.7	59.4	44.0	90.0	87.5	11.6	1.4
4	9.2	6.6	73.2	39.5	89.7	86.4	14.4	1.2
8	9.2	6.6	75.0	29.5	89.9	85.4	14.7	0.9
24	10.2	7.3	114.9	27.5	99.7	95.3	22.5	0.8

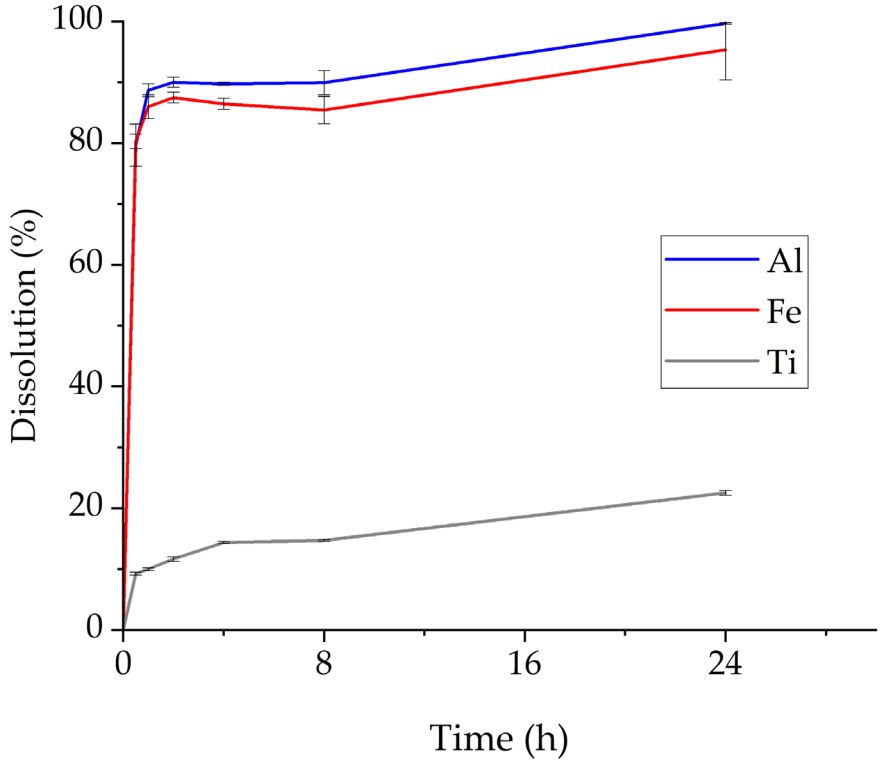

Figure 3. Effect of retention time on the dissolution of Al, Fe, and Ti (pressure: 1 atm, stirring rate: 300 rpm, HCl concentration: 5.9 M, S/L ratio: 5:100 g/mL, temperature: 90 °C, retention time: 24 h).

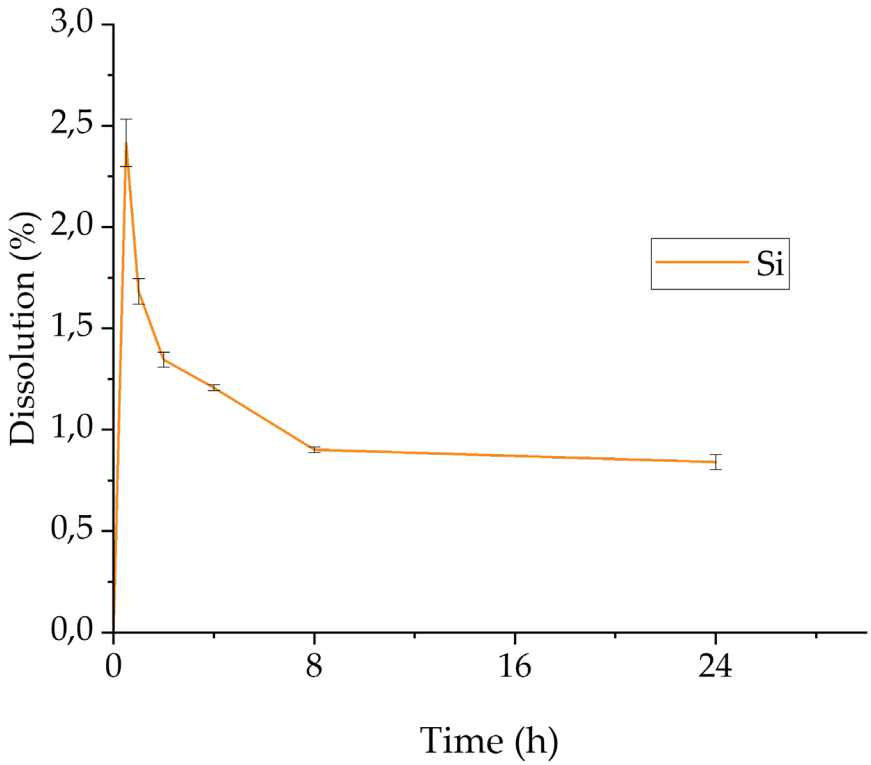

Figure 4. Effect of retention time on the dissolution of Si (stirring rate: 300 rpm, HCl concentration: 5.9 M, S/L ratio: 5:100 g/mL, temperature: 90 °C, retention time: 24 h).

According to Figure 3, Al and Fe show similar leaching behavior with high dissolution rates. More specifically, Fe and Al %wt. dissolution peak during the first hour of leaching

and then remains practically stable until 24 h. At 1 h, the %wt. dissolution value is 86% for Fe and 88.7% for Al. As presented in Figure 2, Al is found mainly in the form of gibbsite, while Fe is included mainly as goethite. Literature data collected and presented by Zhao [49] indicate fast dissolution of Al content from gibbsite with HCl treatment. These data are in full agreement with the presented results. Fe dissolution behavior is also attributed to the fast dissolution of hematite treatment in the aqueous HCl solution [50].

Overall percent weight dissolution of Ti is lower than that of Al and Fe, with a ≈12% dissolution rate noted at 2 h. Ti is found in the form of rutile and anatase, according to Figure 2, which are both stated as slightly soluble in aqueous HCl solutions [51,52].

Moreover, it is worth noting the dissolution behavior of Al, Fe, and Ti in the 8–24 h interval (Figure 3). Almost complete dissolution of Al was achieved at 24 h, while %wt. dissolution of Fe and Ti is increased correspondingly by ≈7% and 10%.

The behavior of Si in the leaching process is depicted in Figure 4. A rapid dissolution of Si in the aqueous HCl solution is observed during the first 30 min of leaching. A maximum value of ≈2.5% wt. dissolution is achieved, corresponding to ≈80 mg/L Si (Table 4). In the period between 30 min and 8 h during leaching, part of the dissolved Si appears to precipitate. The concentration of Si currently decreases from its maximum value of ≈80 mg/L to ≈30 mg/L. The desilication of the solution was effectively achieved at this time and until the end of the leaching test; at 24 h, the concentration of Si remains practically constant. At this point, it must be noted that Si is found, according to the XRD analysis, in the form of quartz (SiO_2), which is known to be insoluble in aqueous HCl under ordinary conditions [53]. Consequently, the source of soluble Si must be attributed to other phases. This point is further discussed in the next section.

To summarize, for the second stage of this study, a value of 2 h retention time is selected as the optimum value for leaching duration, as it combines a high Al dissolution rate (90%) with a low SiO_2/Al_2O_3 mass ratio, calculated to be 0.01.

3.2. Analysis of Leached Residue

The mineralogical characterization of the bauxite tailings' leaching residue at the 5:100 g/mL S/L ratio for a 24 h retention time is presented in Figure 5.

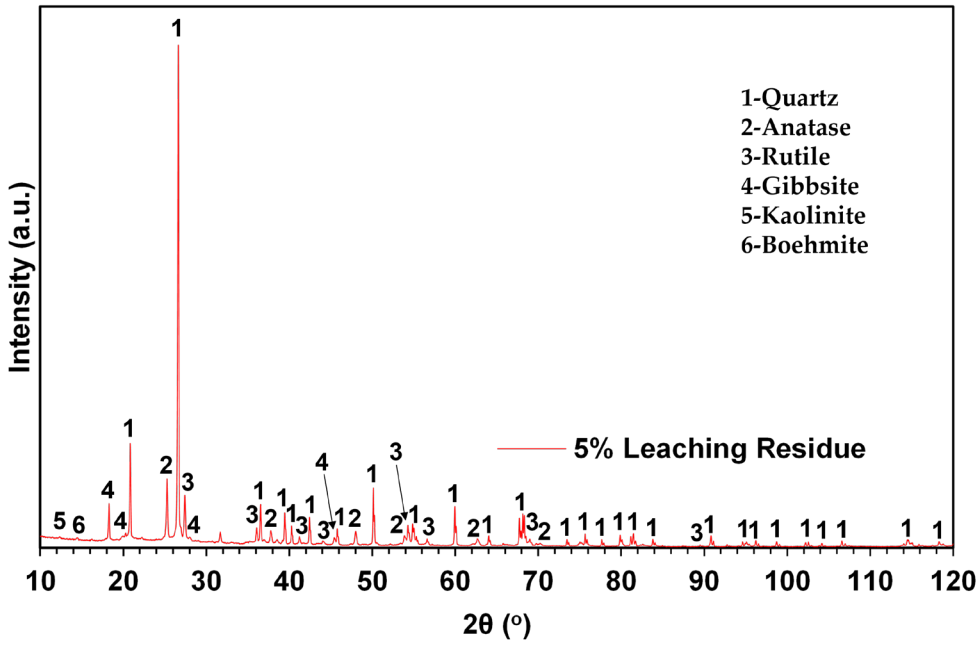

Figure 5. Powder X-ray diffractogram of 5% S/L leaching residue. Legend: 1—Quartz, 2—Anatase, 3—Rutile, 4—Gibbsite, 5—Kaolinite and 6—Boehmite.

Phases included in the analysis of the leaching residue agree with the 24 h PLS metal concentration. More specifically, the nearly complete dissolution of Al and Fe is verified by the existence of the low-intensity peaks of the gibbsite and the elimination of diffraction peaks of the Fe-containing phases. After conducting the 24 h trial, quartz appears as the dominant phase in the residue matrix, as expected by its high concentration in the starting material and the low dissolution rate presented both in Figure 4 and Table 4. Ti is found again in the leaching residue in both the anatase and rutile phases, as expected by the low dissolution rate that was noted. Kaolinite and boehmite, reported in bibliographic data as slightly soluble for the applied conditions [54], were unaffected by the leaching process and traced in the leaching residue.

3.3. Results of the S/L Ratio Optimization Study

Figure 6 depicts the wt.% dissolution of Al and Fe as a function of the S/L ratio in the range 20:100 to 25:100 g/mL (right-hand side axis, solid lines) and their corresponding concentrations in the PLS in g/L (left-hand side axis, dotted lines). Moreover, in Table 5, we report the average %wt. dissolution and concentration for Al, Fe, Ti, and Si in the same range of S/L ratios.

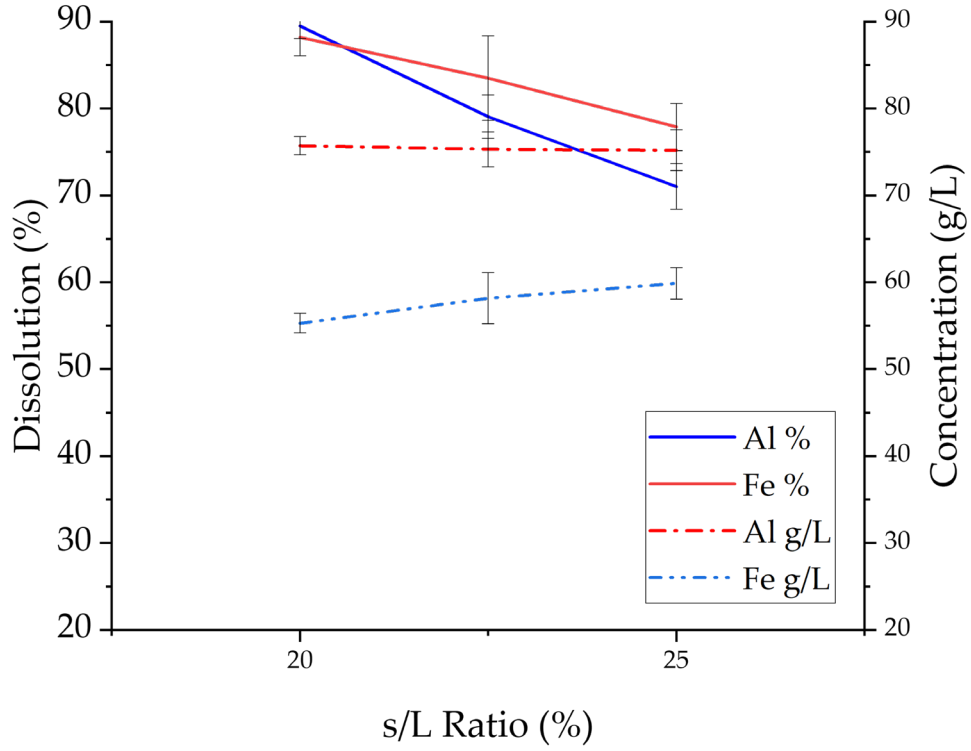

Figure 6. Effect of S/L ratio on the dissolution and concentration of Al and Fe (stirring rate: 300 rpm, HCl concentration: 5.9 M, temperature: 90 °C, retention time: 2 h).

Table 5. Average concentration and %wt. dissolution of Al, Fe, Ti, and Si in the PLS in the range of S/L ratios studied.

S/L (x:100 g/mL)	Average Concentration in PLS				Average %wt. Dissolution in PLS			
	Al (g/L)	Fe (g/L)	Ti (mg/L)	Si (mg/L)	Al	Fe	Ti	Si
20	36.8	25.2	80.4	76.9	89.5	88.2	4.4	0.4
22.5	36.6	26.8	105.8	91.0	79.0	83.5	5.1	0.5
25	36.5	27.8	101.3	102.7	71.0	77.9	4.4	0.5

As expected, based on the results of the 24 h study shown in the previous section, the %wt. dissolution values for Al and Fe are high across the range of S/L values tested. Focusing on the corresponding extraction lines shown in Figure 6, a downward trend can be observed for both Al and Fe. This trend is more pronounced in the case of Al, whereby the decrease in %wt. dissolution is approximately 20%. This decrease in %wt. dissolution is accompanied by a minor increase in the concentration of Fe in the PLS, from 25 g/L in the 20:100 g/mL S/L tests to 28 g/L in the 25:100 g/mL S/L ratio tests. The concentration of Al remains stable across the range of S/L ratio values tested, equal to ≈37 g/L. Nonetheless, free acidity measurements confirmed that there is still an excess of H+ ions for the dissolution of included metallic values, even at the 25:100 g/mL S/L ratio. In more detail, for the 25:100 g/mL S/L ratio tests, free acidity in the produced PLS was calculated to be 0.4 M(pH = 1) while calculated to be 0.5 and 1 M, respectively, for the 22.5:100 and 20:100 g/mL S/L ratio tests. It is therefore highly probable that the observed inability for further dissolution of Al and Fe beyond the 20:100 g/mL S/L value is the result of reaching a solubility limit for these metals in the PLS.

To further validate the view that a solubility limit was reached for this system, the leached residue from the 22.5:100 g/mL S/L ratio test was characterized chemically and mineralogically. The results of the characterizations are presented in Table 6 and Figure 7, respectively.

Table 6. Chemical analysis of the bauxite tailings 22.5:100 g/mL leaching residue sample.

Component	SiO_2	Al_2O_3	Fe_2O_3	TiO_2	LOI	Others
%wt.	35.5 ± 1.1	5.49 ± 0.8	15.5 ± 0.2	4.6 ± 0.1	23.6 ± 0.2	0.4

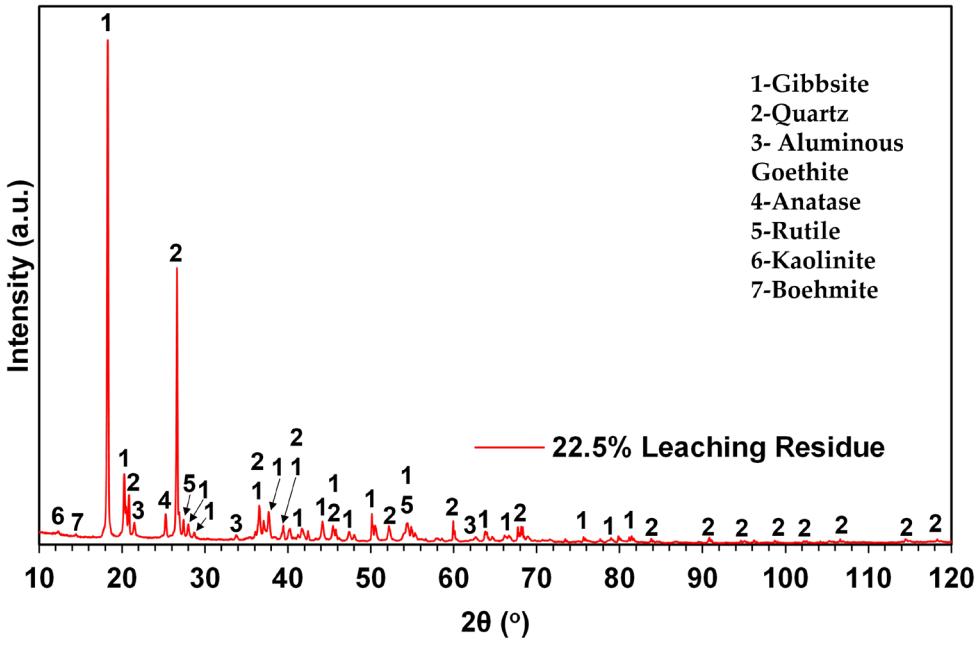

Figure 7. Powder X-ray diffractogram of 22.5% S/L leaching residue. Legend: 1—Gibbsite, 2—Quartz, 3— Aluminous Goethite, 4—Anatase, 5—Rutile, 6—Kaolinite and 7—Boehmite.

The results of the chemical analysis verify that substantial amounts of Al and Fe remain in the leached residue, verifying the results shown in Table 5. Moreover, comparing the diffractogram in Figure 7 with the corresponding diffractogram of the raw material prior to leaching (Figure 2), it can be observed that the leaching process resulted in the complete dissolution of hematite. Gibbsite persists as the main mineral phase, while the remaining crystalline phases observed in the raw material are also present. In addition to

the above, an abrupt increase in the concentration of quartz in the leaching residual material is observed and verified by the significant increase in the intensity of its diffraction peaks.

According to these findings, the 20:100 g/mL S/L value, corresponding to a slight excess of HCl, should be considered the optimum value, leading to a high %wt. dissolution and concentration for Al. Therefore, the initial hypothesis that the excess acidity provided by the hydrolysis of Fe^{3+} and Al^{3+} ions could assist the dissolution of the raw material at increased S/L ratio values was dismissed.

4. Discussion

The efficient acidic leaching of bauxite tailings originating from the Boffa Prefecture, Guinea, for the extraction of Al has been confirmed by the results presented in the present study. By effectively utilizing the technology developed in the framework of the AlSiCal project, an acceptable Al-bearing chloride solution was produced, which could be utilized downstream for the precipitation of $AlCl_3 \cdot 6H_2O$. As the experimental study was divided into two sections, i.e., the 24 h leaching study and the S/L ratio optimization tests, this section addresses correspondingly the main findings and observations made at each stage of the work.

4.1. Leachability of Major Compounds in Bauxite Tailings

The 24 h leaching trials were conducted to monitor the dissolution profile for the major elements Al, Fe, Ti, and Si. Al and Fe were expected to exhibit increased %wt. dissolution in aqueous HCl, while the opposite was expected for Ti and Si. Especially for the case of Si, its behavior in the leaching process is a crucial parameter, as precipitated SiO_2 from acidic solutions can form gels. The occurrence of SiO_2 gel formation can constitute the separation of the leached residue from the PLS impossible.

The 24 h study confirmed the rapid and efficient dissolution of both Al and Fe. More specifically, literature data collected and presented by Zhao [49] confirm the fast dissolution of Al from gibbsite when leaching with aqueous HCl. Those data are in full agreement with the results presented in this study (see dissolution results for Al in Table 4 and leached residue XRD analysis in Figure 5). Concerning the leachability of the minor Al-bearing phases, as depicted in Figure 5, boehmite and kaolinite are virtually unaffected by the leaching process, as proposed bibliographically by Bénézeth [55] and Terry [56].

The high %wt. dissolution values for Fe presented in Figure 3 and the data in Table 4, combined with the XRD analysis of the leached residue (Figure 5), suggest that during the leaching trials, hematite and goethite were almost totally dissolved. During the treatment with aqueous hydrochloric acid (HCl) solutions, hematite exhibits a faster dissolution rate per unit area compared to goethite. This disparity in rates appears to persist throughout the entire dissolution reaction, as supported by qualitative evidence. Similarly, when mixtures of goethite and hematite are present, all the hematite dissolves before goethite, even when the former compound is present in excess [57,58]. Based on these remarks, it could be assumed that residual undissolved Fe is found in the form of goethite. However, no clear peak was found in the residual matrix. This indicates the possibility for the presence of Fe in some of the undissolved minerals in the raw material.

Ti dissolution rates observed do not agree with the bibliographic data that demonstrate anatase and rutile are slightly soluble in HCl treatment. The dissolved Ti content could be linked to the existence of a soluble Ti source. This source could be in the matrix of detected mineralogical phases or amorphous material. Data provided by Valeton [59], Hartman [60], and Vind [61] suggest that Ti, except for the form of rutile, the most common and stable phase in bauxites, could be found through the diagenetic process to anatase and Fe-minerals. Ti substitution in hematite could codissolve with Fe and explains the dissolution rates observed. Indeed, Trolard et al. [62] have studied the existence of trace elements in iron oxides originating from lateritic mineralization processes and confirmed the substitution of Ti for Fe in hematite up to 2% w/w. On the other hand, according to the same research group, Ti cannot substitute for Fe in goethite. Concerning the second

observed TiO_2 phase of anatase, Schwertmann et al. [63] have confirmed the isomorphous replacement of Ti by Fe, by the increase in the unit cell parameters *a* and *V* with increasing Fe content. The replacement of Ti by Fe in anatase was also supported by Mössbauer and EPR spectra. Consequently, the incomplete dissolution of Fe could be attributed to the substitution of Ti by Fe in the anatase structure.

A similar unexpected dissolution but to a smaller degree was noted also in the case of Si. Si in the form of quartz is known to be insoluble in aqueous HCl solution under atmospheric pressure conditions [64,65]. However, Si dissolution is noted. This phenomenon could be linked with the existence of Si in the amorphous mass calculated during the raw material XRD analysis. This statement is endorsed also by the Si concentration differences between chemical analysis and XRD quantitative analysis. Amorphous Si phases are reported as easily soluble in HCl treatment [66]. The extent of Si dissolution is not severe and indeed no SiO_2 gelation phenomena were observed, although most of the dissolved Si precipitates, as shown in Figure 4.

4.2. Optimization of S/L Ratio

The goal of the S/L ratio optimization trials was to utilize the highest feasible S/L ratio in a one-stage leaching process and to produce a concentrated Al-containing solution, suitable for the subsequent precipitation of Al in the form of chloride salts. Analysis of the results showed that a further rise in the S/L ratio over the 20:100 g/mL value did not affect positively the process, as depicted in Figure 6. However, trials using higher S/L ratio values provided useful information about the overall process.

The hypothesis tested in these trials was that the hydrolysis of the trivalent ions (Al^{3+} and Fe^{3+}) generates additional acidity to the system, which could potentially lead to increased %wt. extraction for Al. As stated in previous works [67], through the dissolution of gibbsite-bearing materials and in the absence of any complexing species, Al concentration in the final produced solution is controlled by the dissolution of gibbsite (presented in Equation (2)) and the hydrolysis of Al^{3+} (presented in Equation (6)). Free acidity measurements confirmed the hydrolysis theory as free acidity was found in all produced solutions. Thus, the decrease in %wt. extraction noted for Al and Fe could not be linked with the lack of acidity but with the reach of a solubility limit for the system under investigation. With the reach of this limit, any further dissolution is not possible, as confirmed by the XRD analysis of the residue from the 25:100 g/mL S/L ratio tests (Figure 7), showing that gibbsite and Al-goethite remain partially insoluble after 2 h of treatment. Compared to the solubility of Al in the $AlCl_3$-HCl-H_2O system, the observed solubility of Al in this study is, as expected, lower [68]. This deviation can be explained by the high concentration of other dissolved impurities and more particularly, Fe. As presented by Cheng et al. [69], Al^{3+} solubility is decreased by the increase in Fe^{3+} concentration and density. This relationship could also explain the small drop in Al concentration with the rise in Fe concentration noted with the rise in the S/L ratio, as shown in Table 5.

The work portrayed above describes a method to produce an $AlCl_3$-$FeCl_3$ solution containing approximately 37 g/L Al and 25 g/L Fe. This solution could be treated based on AlSiCal's technology for Al_2O_3 production, as it is depicted in Figure 1. The PLS produced in the study can be effectively treated downstream by an HCl-purging crystallization process, leading to the precipitation of the corresponding hydrated chloride. A tailored selection of applied conditions employed during the process can prevent the coprecipitation of undesired impurities [70]. As stated by Cheng et al. [69], Al precipitation in the form of hydrated salt is preferred over Fe at ambient temperature, which is the major impurity in the produced solution. The solubility of Fe is almost unchanged under elevated HCl concentrations. Moreover, utilizing a temperature above 60 °C would hinder the precipitation of iron (Fe) [71]. Additionally, purification cycles could be repeated multiple times until the desired level of purity, as per the established criteria, is achieved. Known techniques could be applied for HCl regeneration [72] from the spent acid solution. Finally, the Fe-rich

solution, after the removal of the Ti impurities, can be harnessed as $FeCl_3$, a commercially valuable product.

5. Conclusions

The goal of the present research was to access BTs as an alternative source for the Al_2O_3 industry. The composition of this waste necessitates an acid treatment for the dissolution of Al and its separation from Si content. In more detail, the following results were shown:

- A 24 h leaching trial with an aqueous 5.9 M HCl solution and a 5:100 g/mL S/L ratio led to almost total Al dissolution and Fe dissolution and the production of a predominant siliceous residue. PLS calculated impurities were 27.5 ppm Si and 114.9 ppm Ti.
- Two-hour duration was selected as the optimum leaching time combining high Al dissolution rates and low Si dissolution.
- The S/L ratio optimization study was performed with the same leaching conditions as in the 24 h study (stirring rate: 300 rpm, HCl concentration: 5.9 M, temperature: 90 °C), but with a 2 h duration. The range in S/L ratio values tested was 20:100–25:100 g/mL, corresponding from a slight excess of acid to an excess of solids. The 20% S/L ratio proved to be the optimum, leading to the production of a solution with 36.8 g/L Al, 25.2 g/L Fe, 80.4 ppm Ti, and 76.9 ppm Si.
- Further increase in the S/L ratio value led to a decrease in Al %wt. extraction, which is most likely attributed to reaching the solubility limit for this system.
- In all of the S/L ratios tested, filtering of the leached residue was conducted with no difficulties.

To conclude, BTs are a promising material for alternative Al_2O_3 extraction and future work should focus on the valorization of the major byproducts, i.e., the SiO_2-rich residue and the $FeCl_3$ content of the PLS.

Author Contributions: Conceptualization, M.B., M.V. and D.P.; methodology, M.V. and M.B.; validation, M.V., A.P. and D.K.; data curation, M.B. and A.P.; writing—original draft preparation, M.B. and D.K.; writing—review and editing, M.V. and E.B.; supervision, D.P. All authors have read and agreed to the published version of the manuscript.

Funding: The research leading to these results received funding from the European Union's Horizon 2020 research and innovation program AlSiCal under grant agreement number 820911.

Institutional Review Board Statement: Not applicable.

Informed Consent Statement: Not applicable.

Data Availability Statement: No new data were created or analyzed in this study. Data sharing is not applicable to this article.

Acknowledgments: Material used in this study was provided by Anastasios Kladis on behalf of AdMiRIS.

Conflicts of Interest: The authors declare no conflict of interest.

References

1. Aluminium. Global Energy Transitions Stocktake. 2023 11/07/2023. Available online: https://www.iea.org/energy-system/industry/aluminium#tracking (accessed on 2 November 2023).
2. Brough, D.; Jouhara, H. The aluminium industry: A review on state-of-the-art technologies, environmental impacts and possibilities for waste heat recovery. *Int. J. Thermofluids* **2020**, *1–2*, 100007. [CrossRef]
3. Sverdrup, H.U.; Ragnarsdottir, K.V.; Koca, D. Aluminium for the future: Modelling the global production, market supply, demand, price and long term development of the global reserves. *Resour. Conserv. Recycl.* **2015**, *103*, 139–154. [CrossRef]
4. Elshkaki, A.; Lei, S.; Chen, W.-Q. Material-energy-water nexus: Modelling the long term implications of aluminium demand and supply on global climate change up to 2050. *Environ. Res.* **2019**, *181*, 108964. [CrossRef]
5. Liu, G.; Bangs, C.E.; Müller, D.B. Stock dynamics and emission pathways of the global aluminium cycle. *Nat. Clim. Chang.* **2012**, *3*, 338–342. [CrossRef]
6. Meyer, F.M. Availability of Bauxite Reserves. *Nat. Resour. Res.* **2004**, *13*, 161–172. [CrossRef]

7. European Commission. *Study on the Critical Raw Materials for the EU 2023—Final Report*; Publications Office of the European Union; European Commission: Brussels, Belgium, 2023.
8. Burton, J. *2022 Final List of Critical Minerals*; U.S. Geological Survey: Reston, VA, USA, 2021.
9. Government of Canada. The Canadian Critical Minerals Strategy From Exploitation To Recycling: Powering the Green and Digital Economy for Canada and the World. Available online: Canada.ca (accessed on 9 September 2023).
10. Habashi, F. *Handbook of Extractive Metallurgy*; Wiley–VCH: Hoboken, NJ, USA, 1998; Volume 2.
11. Shen, X.; Ma, D.; Guo, M.; Zhang, M. Efficient removal of K_2O and Fe_2O_3 impurities from bauxite tailings through active calcination combined with acid leaching. *Can. Metall. Q.* **2017**, *56*, 294–300. [CrossRef]
12. Traoré, D.; Traoré, S.; Diakité, S. Bauxite industry in guinea and value opportunities of the resulting red mud as residue for chemical and civil engineering purposes. *J. Civ. Eng. Res.* **2014**, *4*, 14–24.
13. Komlóssy, G.; Van Deursen, C.; Raahauge, B.E. *Bauxite: Geology, Mineralogy, Resources, Reserves and Beneficiation*; Springer International Publishing: Berlin/Heidelberg, Germany, 2022; pp. 19–132.
14. Datta, B.; Nandi, A. *Bauxite Beneficiation: An Approach to Value Addition in Mining*; Springer International Publishing: Berlin/Heidelberg, Germany, 2021; pp. 99–114.
15. Bagherzadeh, Y.; Golmakani, M.; Karimi, E. Straight synthesis of α and γ alumina from kaolin by HCl acid leaching. *J. Min. Metall. Sect. B Metall.* **2023**, 17. [CrossRef]
16. Tantawy, M.A.; Alomari, A.A. Extraction of alumina from Nawan kaolin by acid leaching. *Orient. J. Chem.* **2019**, *35*, 1013. [CrossRef]
17. Valeev, D.; Shoppert, A.; Mikhailova, A.; Kondratiev, A. Acid and Acid-Alkali Treatment Methods of Al-Chloride Solution Obtained by the Leaching of Coal Fly Ash to Produce Sandy Grade Alumina. *Metals* **2020**, *10*, 585. [CrossRef]
18. Valeev, D.V.; Mansurova, E.R.; Bychinskii, V.A.; Chudnenko, K.V. Extraction of Alumina from high-silica bauxite by hydrochloric acid leaching using preliminary roasting method. In *IOP Conference Series: Materials Science and Engineering*; IOP publishing: Bristol, UK, 2016; Volume 110, p. 012049.
19. Zhao, A.; Zhang, T.; Lv, G. Acid Leaching Performance of Gibbsite-type Bauxite with High Iron Content. *Multipurp. Util. Miner. Resour.* **2022**, *1*, 173–178.
20. Aranda, A.; Mastin, J. Alumina and Carbonate Production Method from Al-rich Materials with Integrated CO_2 Utilization. European Patent EP3148935B1, 11 March 2015.
21. Neron, T.; Cassayre, L.; Zhuo, X.; Manero, M.-H.; Bourgeois, F.; Billet, A.-M.; Julcour, C. Thermo-kinetic modelling of the acidic leaching of anorthosite: Key learnings toward the conception of a sustainable industrial process. *Miner. Eng.* **2022**, *180*, 107500. [CrossRef]
22. Bagani, M.; Balomenos, E.; Panias, D. Exploitation of Kaolin as an Alternative Source in Alumina Production. *Mater. Proc.* **2021**, *5*, 24.
23. Bagani, M.; Balomenos, E.; Panias, D. Nepheline Syenite as an Alternative Source for Aluminum Production. *Minerals* **2021**, *11*, 734. [CrossRef]
24. Wang, Y.; Lan, Y.; Hu, Y. Adsorption mechanisms of Cr(VI) on the modified bauxite tailings. *Miner. Eng.* **2008**, *21*, 913–917. [CrossRef]
25. Dong, Y.; Feng, N.X.; Wang, Y.W.; Wu, X.L. Preparation of primary Al-Si alloy from bauxite tailings by carbothermal reduction process. *Trans. Nonferrous Met. Soc. China* **2010**, *20*, 147–152.
26. Ma, D.; Wang, Z.; Guo, M.; Zhang, M.; Liu, J. Feasible conversion of solid waste bauxite tailings into highly crystalline 4A zeolite with valuable application. *Waste Manag.* **2014**, *34*, 2365–2372. [CrossRef]
27. Lei, P.-C.; Shen, X.-J.; Li, Y.; Guo, M.; Zhang, M. An improved implementable process for the synthesis of zeolite 4A from bauxite tailings and its Cr^{3+} removal capacity. *Int. J. Miner. Met. Mater.* **2016**, *23*, 850–857. [CrossRef]
28. Qiang, Z.; Shen, X.; Guo, M.; Cheng, F.; Zhang, M. A simple hydrothermal synthesis of zeolite X from bauxite tailings for highly efficient adsorbing CO2 at room temperature. *Microporous Mesoporous Mater.* **2019**, *287*, 77–84. [CrossRef]
29. Yang, N.; Gou, L.; Bai, Z.; Cheng, F.; Guo, M.; Zhang, M. A Simple and Mild Synthesis of Zeolite Y from Bauxite Tailings for Lead Adsorption: Reusable, Efficient and Highly Selective. *J. Inorg. Organomet. Polym. Mater.* **2022**, *32*, 3496–3507. [CrossRef]
30. Peng, Y.; Jiang, J.; Ou, X.; Qin, J. Investigating the Properties of Foamed Mixture Lightweight Soil Mixed with Bauxite Tailings as Filler. *Adv. Mater. Sci. Eng.* **2019**, *2019*, 6295348. [CrossRef]
31. Peng, Y.; Ou, X.; Chen, X.; Lin, X.; Shen, X. Utilization of discarded bauxite tailings into eco-friendly foamed mixture lightweight soil. *J. Clean. Prod.* **2022**, *333*, 130167. [CrossRef]
32. Yang, L.; Ma, X.; Hu, X.; Liu, J.; Wu, Z.; Shi, C. Production of lightweight aggregates from bauxite tailings for the internal curing of high-strength mortars. *Constr. Build. Mater.* **2022**, *341*, 127800. [CrossRef]
33. Ren, Y.; Ren, Q.; Wu, X.; Zheng, J.; Hai, O. Mechanism of low temperature sintered high-strength ferric-rich ceramics using bauxite tailings. *Mater. Chem. Phys.* **2019**, *238*, 121929. [CrossRef]
34. Zhang, Y.; Zhang, J.; Wu, L.; Tan, L.; Xie, F.; Cheng, J. Extraction of lithium and aluminium from bauxite mine tailings by mixed acid treatment without roasting. *J. Hazard. Mater.* **2021**, *404*, 124044. [CrossRef] [PubMed]
35. AlSiCal. 2023. Available online: https://www.alsical.eu/ (accessed on 9 November 2023).
36. Gates-Rector, S.; Blanton, T. The Powder Diffraction File: A quality materials characterization database. *Powder Diffr.* **2019**, *34*, 352–360. [CrossRef]

37. Cheary, R.W.; Coelho, A.A. A fundamental parameters approach to X-ray line-profile fitting. *J. Appl. Crystallogr.* **1992**, *25*, 109–121. [CrossRef]
38. Järvinen, M. Application of symmetrized harmonics expansion to correction of the preferred orientation effect. *J. Appl. Crystallogr.* **1993**, *26*, 525–531. [CrossRef]
39. Schulz, D.G. The Influence of Aluminum on Iron Oxides. VIII. Unit-Cell Dimensions of Al-Substituted Goethites and Estimation of Al from them. *Clays Clay Miner.* **1984**, *32*, 36–44. [CrossRef]
40. Schwertmann, U.; Carlson, L. Aluminum Influence on Iron Oxides: XVII. Unit-Cell Parameters and Aluminum Substitution of Natural Goethites. *Soil Sci. Soc. Am. J.* **1994**, *58*, 256–261. [CrossRef]
41. Wells, M.A.; Gilkes, R.J.; Anand, R.R. The formation of corundum and aluminous hematite by the thermal dehydroxylation of aluminous goethite. *Clay Miner.* **1989**, *24*, 513–530. [CrossRef]
42. Fazey, P.G.; O'Connor, B.H.; Hammond, L.C. X-Ray Powder Diffraction Rietveld Characterization of Synthetic Aluminum-Substituted Goethite. *Clays Clay Miner.* **1991**, *39*, 248–253. [CrossRef]
43. Fontes, M.P.F.; Weed, S.B. Iron Oxides in Selected Brazilian Oxisols: I. Mineralogy. *Soil Sci. Soc. Am. J.* **1991**, *55*, 1143–1149. [CrossRef]
44. Aylmore, M.G.; Walker, G.S. The quantification of lateritic bauxite minerals using X-ray powder diffraction by the Rietveld method. *Powder Diffr.* **1998**, *13*, 136–143. [CrossRef]
45. Gan, B.K.; Taylor, Z.; Xu, B.; van Riessen, A.; Hart, R.D.; Wang, X.; Smith, P. Quantitative phase analysis of bauxites and their dissolution products. *Int. J. Miner. Process.* **2013**, *123*, 64–72. [CrossRef]
46. Negrão, L.B.A.; Pöllmann, H.; Alves, T.K.C. Mineralogical Appraisal of Bauxite Overburdens from Brazil. *Minerals* **2021**, *11*, 677. [CrossRef]
47. Negrão, L.B.A.; da Costa, M.L.; Pöllmann, H.; Horn, A. An application of the Rietveld refinement method to the mineralogy of a bauxite-bearing regolith in the Lower Amazon. *Miner. Mag.* **2018**, *82*, 413–431. [CrossRef]
48. O'Connor, B.H.; Raven, M.D. Application of the Rietveld Refinement Procedure in Assaying Powdered Mixtures. *Powder Diffr.* **1988**, *3*, 2–6. [CrossRef]
49. Zhao, A.-C.; Liu, Y.; Zhang, T.-A.; Lü, G.-Z.; Dou, Z.-H. Thermodynamics study on leaching process of gibbsitic bauxite by hydrochloric acid. *Trans. Nonferrous Met. Soc. China* **2013**, *23*, 266–270. [CrossRef]
50. Schwertmann, U. Solubility and dissolution of iron oxides. *Plant Soil* **1991**, *130*, 1–25. [CrossRef]
51. Lanyon, M.R.; Lwin, T.; Merritt, R.R. The dissolution of iron in the hydrochloric acid leach of an ilmenite concentrate. *Hydrometallurgy* **1999**, *51*, 299–323. [CrossRef]
52. Yang, M.-H.; Chen, P.-C.; Tsai, M.-C.; Chen, T.-T.; Chang, I.-C.; Chiu, H.-T.; Lee, C.-Y. Anatase and brookite TiO_2 with various morphologies and their proposed building block. *CrystEngComm* **2013**, *16*, 441–447. [CrossRef]
53. Knauss, K.G.; Wolery, T.J. The dissolution kinetics of quartz as a function of pH and time at 70 °C. *Geochim. Cosmochim. Acta* **1988**, *52*, 43–53. [CrossRef]
54. Peryea, F.J.; Kittrick, J.A. Relative Solubility of Corundum, Gibbsite, Boehmite, and Diaspore at Standard State Conditions. *Clays Clay Miner.* **1988**, *36*, 391–396. [CrossRef]
55. Bénézeth, P.; Palmer, D.A.; Wesolowski, D.J. Dissolution/precipitation kinetics of boehmite and gibbsite: Application of a pH-relaxation technique to study near-equilibrium rates. *Geochim. Cosmochim. Acta* **2008**, *72*, 2429–2453. [CrossRef]
56. Terry, B. The acid decomposition of silicate minerals part I. Reactivities and modes of dissolution of silicates. *Hydrometallurgy* **1983**, *10*, 135–150. [CrossRef]
57. Cornell, R.M.; Giovanoli, R. Acid Dissolution of Hematites of Different Morphologies. *Clay Miner.* **1993**, *28*, 223–232. [CrossRef]
58. Voelz, J.L.; Johnson, N.W.; Chun, C.L.; Arnold, W.A.; Penn, R.L. Quantitative Dissolution of Environmentally Accessible Iron Residing in Iron-Rich Minerals: A Review. *ACS Earth Space Chem.* **2019**, *3*, 1371–1392. [CrossRef]
59. Valeton, I. *Bauxites*; Elsevier: Amsterdam, The Netherlands, 2010.
60. Hartman, J.A. The titanium mineralogy of certain bauxites and their parent materials. *Econ. Geol.* **1959**, *54*, 1380–1405. [CrossRef]
61. Vind, J.; Malfliet, A.; Bonomi, C.; Paiste, P.; Sajó, I.E.; Blanpain, B.; Tkaczyk, A.H.; Vassiliadou, V.; Panias, D. Modes of occurrences of scandium in Greek bauxite and bauxite residue. *Miner. Eng.* **2018**, *123*, 35–48. [CrossRef]
62. Trolard, F.; Bourrie, G.; Jeanroy, E.; Herbillon, A.J.; Martin, H. Trace metals in natural iron oxides from laterites: A study using selective kinetic extraction. *Geochim. Cosmochim. Acta* **1995**, *59*, 1285–1297. [CrossRef]
63. Schwertmann, U. Iron Substitution in Soil and Synthetic Anatase. *Clays Clay Miner.* **1995**, *43*, 599–606. [CrossRef]
64. Gutberlet, T.; Hilbig, H.; Beddoe, R. Acid attack on hydrated cement—Effect of mineral acids on the degradation process. *Cem. Concr. Res.* **2015**, *74*, 35–43. [CrossRef]
65. Dietzel, M. Dissolution of silicates and the stability of polysilicic acid. *Geochim. Cosmochim. Acta* **2000**, *64*, 3275–3281. [CrossRef]
66. Alexander, G.B.; Heston, W.M.; Iler, R.K. The Solubility of Amorphous Silica in Water. *J. Phys. Chem.* **1954**, *58*, 453–455. [CrossRef]
67. Ridley, M.K.; Wesolowski, D.J.; Palmer, D.A.; Bénézeth, P.; Kettler, R.M. Effect of Sulfate on the Release Rate of Al^{3+} from Gibbsite in Low-Temperature Acidic Waters. *Environ. Sci. Technol.* **1997**, *31*, 1922–1925. [CrossRef]
68. Brown, R. *Solubility and Activity of Aluminium Chloride in Aqueous Hydrochloric Acid Solutions*; US Bureau of Mines: Pittsburg, PA, USA, 1979.
69. Cheng, H.; Wu, L.; Cao, L.; Zhao, J.; Xue, F.; Cheng, F. Phase Diagram of AlC_{l3}–$FeCl_3$–H_2O (− HCl) Salt Water System at 298.15 K and Its Application in the Crystallization of $AlCl_3 \cdot {}_6H_2O$. *J. Chem. Eng. Data* **2019**, *64*, 5089–5094. [CrossRef]

70. Noble, E.G.; Shanks, D.E.; Bauer, D.J. *Solubilities of Chloride Salts of Alkali and Alkaline-Earth Metals when Sparged with Hydrogen Chloride*; US Department of the Interior, Bureau of Mines: Pittsburg, PA, USA, 1985; Volume 8991.
71. Maysilles, J.H.; Traut, D.E.; Sawyer, D.L. *Aluminum Chloride Hexahydrate Crystallization by HC1 Gas Sparging*; US Department of the Interior, Bureau of Mines: Pittsburg, PA, USA, 1982; Volume 8590.
72. Pérez-Ramírez, J.; Mondelli, C.; Schmidt, T.; Schlüter, O.F.-K.; Wolf, A.; Mleczko, L.; Dreier, T. Sustainable chlorine recycling via catalysed HCl oxidation: From fundamentals to implementation. *Energy Environ. Sci.* **2011**, *4*, 4786–4799. [CrossRef]